Plasma and Cavitation Dynamics during Pulsed Laser Microsurgery *in vivo*

M. Shane Hutson* and Xiaoyan Ma

Department of Physics & Astronomy, Vanderbilt University, VU Station B #351807, Nashville, Tennessee 37235-1807, USA

(Received 21 May 2007; published 10 October 2007)

We compare the plasma and cavitation dynamics underlying pulsed laser microsurgery in water and in fruit fly embryos (*in vivo*)—specifically for nanosecond pulses at 355 and 532 nm. We find two key differences. First, the plasma-formation thresholds are lower *in vivo* —especially at 355 nm—due to the presence of endogenous chromophores that serve as additional sources for plasma seed electrons. Second, the biological matrix constrains the growth of laser-induced cavitation bubbles. Both effects reduce the disrupted region *in vivo* when compared to extrapolations from measurements in water.

DOI: 10.1103/PhysRevLett.99.158104 PACS numbers: 87.80.−y, 47.55.dp, 52.38.Mf, 52.50.Jm

Pulsed laser microsurgery has emerged as an important technique for probing biological systems through the targeted disruption of cellular and subcellular structures [1,2]. Applications include cell lineage studies in developing organisms [3], sampling of heterogeneous systems via laser pressure catapulting [4], and gene delivery through transient membrane disruption (optoporation) [5]. Additionally, new applications have focused on the dissection of cytoskeletal filaments—either as probes of intracellular forces in adherent cells [6] or of intercellular forces in developing embryos [7]. Even with an abundance of applications, there have been just a few attempts to characterize the underlying physical mechanisms [8,9]. Recent work has provided crucial clues that both fs- and ns-pulsed laser microsurgery are driven by laser-induced plasma formation [10,11]. The expanding plasma subsequently drives shock wave propagation and the dynamic expansion of cavitation bubbles. One of the most puzzling findings from these studies was that cavitation bubbles from ns pulses reached radii of 45–470 μm. Under optimal conditions in living tissues, the laser-disrupted region is just a few hundred nm [2].

This conflict points to a limitation in our physical understanding of pulsed laser microsurgery. The initial studies were conducted only in distilled water—and only at visible and near-IR wavelengths. Since water is the dominant component (by weight) of most biological tissues, these studies are highly relevant; however, real tissues differ from distilled water in both mechanical and electronic properties. Most tissues are viscoelastic; and although pure water is well-approximated as an amorphous semiconductor, tissues contain many molecules with energy levels inside the 6.5 eV water band gap. Such defects are present at low concentrations, but may play a large role in plasma formation—particularly at near-UV wavelengths where they can directly absorb laser energy. No one has systematically explored the impact of the viscoelastic biological matrix or the role of endogenous chromophores. In this Letter, we address these issues by comparing the plasma and cavitation dynamics during ns–laser microsurgery in water to that in living fruit fly embryos (*in vivo*)—both at visible and near-UV wavelengths.

We focus either the second or third harmonic (532 or 355 nm) of a Q-switched Nd:YAG laser (4 ns pulse width) through the 40 ×, 1.3 NA oil-immersion objective of a Zeiss LSM410 inverted confocal microscope. The entire laser-microsurgery system has been described in detail previously [12] and can take fluorescent images of thick biological samples while simultaneously cutting the samples with single (or multiple) pulses at any user-defined location (or trajectory). The transgenic fruit flies used in these experiments produce a green fluorescent protein: E-cadherin chimera that fluorescently labels epithelial cell borders [13]. The fruit fly embryos are approximately ellipsoidal (~500 by 200 μm) and are arranged on a coverslip with their long axis parallel to the surface. The fly embryos are covered with distilled water and a needle hydrophone (Onda, 0.5 mm aperture, <20 ns rise time, 2.24 V/MPa sensitivity) is placed 1.5 mm above the targeted embryo to record the pressure transients associated with plasma formation, i.e., shock wave propagation and cavitation bubble collapse. The time between these two transients is a direct measure of the cavitation bubble oscillation time, T_{osc}. The presence or absence of a shock wave transient is used to quantify plasma-formation thresholds (by fitting the probabilities to a Gaussian error function [14]). All thresholds had minimal shock wave amplitudes of at least 6× the noise-equivalent pressure (0.4 kPa). For 532 nm ablation, this method and plasma luminescence yield identical thresholds. Luminescence cannot be used *in vivo* at 355 nm due to strong autofluorescence.

Figure 1 shows how strongly the *in vivo* effects of laser microsurgery depend on wavelength. At 532 nm, with an energy just above the plasma-formation threshold, our attempt to cut a single cell edge in a fly embryo destroyed all cellular structure over a wide area (>80 μm in diameter). At 355 nm, and 5× threshold, we disrupted just the targeted cell edge. The two cells sharing this edge then expand over tens of seconds as the fly epithelium comes to

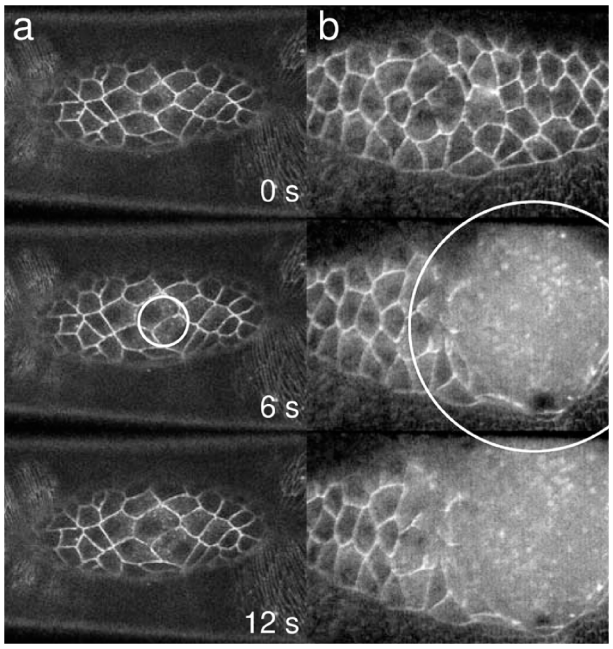

FIG. 1. Assessment of cavitation damage *in vivo*. Three sequential confocal images are shown of fruit fly embryos before and after ablation at (a) $\lambda = 355$ nm and $E_P = 1.22$ μJ, i.e., 5× threshold, or (b) $\lambda = 532$ nm and $E_P = 8.26$ μJ, i.e., 1× threshold. Ablation occurred between the first two images. Each white circle is centered on the ablation site with a radius equal to the calculated $R_{max} = 12.9$ μm in (a) and 65.6 μm in (b).

a new mechanical equilibrium. Strong clues as to the root of these differences come from simultaneous hydrophone measurements. The measured T_{osc} can be used to calculate the maximum bubble radius (R_{max}) after Rayleigh [15]. Although this equation is not strictly valid for small bubbles (due to its neglect of surface tension) or *in vivo* (a viscoelastic medium that lacks spherical symmetry), our direct observations (below) show that a predicted R_{max} is good to within ±15%. In these two examples, R_{max} was 5× larger in the 532 nm ablation—matching the much larger disrupted region.

The differences in R_{max} above are a direct consequence of large differences in the plasma-formation threshold *in vivo*. In distilled water, the plasma-formation thresholds at 355 and 532 nm were 1.86 and 13.28 μJ, respectively. This 532 nm threshold is considerably higher than previously reported [10] due to known sources of spherical aberration in our beam line [16]. Nonetheless, the sevenfold increase at the longer wavelength is consistent with previous comparisons [10]. Surprisingly, we find even larger differences *in vivo*, where the thresholds at 355 and 532 nm were 0.23 and 8.63 μJ, respectively—a 38-fold increase at the longer wavelength. This large difference is mainly due to the fact that the *in vivo* threshold at 355 nm is just 1/8 of the threshold in water.

Once above threshold, the subsequent cavitation dynamics are not strongly wavelength dependent. Measurements of T_{osc} (and R_{max}) for a wide range of pulse energies at both 355 and 532 nm are shown in Fig. 2. The most striking feature of this plot is that all measurements in water (filled symbols) fall along a single curve. This includes data previously reported by others for 532 and 1064 nm [10]. Similarly, almost all measurements *in vivo* (open symbols) fall along a different single curve—one with smaller bubble radii. The few exceptions are for high energy ablations at 532 nm conducted after the vitelline membrane encasing a fly embryo was ruptured by an earlier pulse. These points fall along the curve describing cavitation dynamics in water, suggesting that the main difference between the "in-water" and *in vivo* curves is mechanical constraint of the cavitation bubbles. In accord with this explanation, the *in vivo* cavitation bubbles plateau at high energies with an R_{max} just below 70 μm, but the bubbles in water continue to grow. The smallest cavitation bubbles are observed at the 355 nm *in vivo* threshold with an R_{max} of just 3.2 μm.

What then accounts for the much smaller threshold at 355 nm and *in vivo*? The plasma-formation threshold for ns pulses is largely determined by the intensity needed to produce quasifree seed electrons—by multiphoton ionization in pure water—with subsequent formation of the full plasma through cascade ionization [17]. To lower the threshold, we need a new source of seed electrons. Added chromophores are known to lower the plasma threshold for dried samples and fs pulses [18]. In such cases, multiphoton ionization of the chromophore can compete with that of residual water because the concentrations are similar. In wet samples like ours, any new source will be at a much lower concentration than water, so its ionization cross section must be correspondingly larger. Our primary candidate is the reduced form of nicotinamide adenine dinucleotide (NADH). This ubiquitous biomolecule is present in relatively high (mM) concentra-

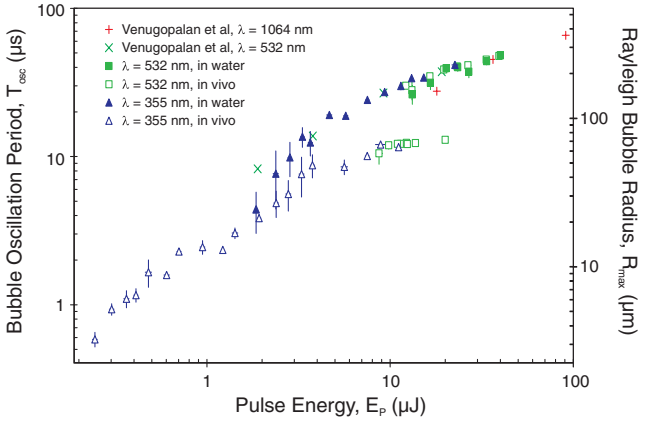

FIG. 2 (color online). Cavitation bubble parameters versus laser pulse energy in water and *in vivo*. To facilitate comparison, we have included data previously reported for ablation in water at 532 and 1064 nm [10].

tions in developing embryos [19]; it has a strong and broad absorption maximum at 340 nm [20]; and it has been shown to undergo one-electron oxidation when irradiated at 353 nm by a sequential two-photon process [21]. As opposed to a multiphoton process, this sequential two-photon ionization could generate seed electrons at much lower intensities. To test this hypothesis, we irradiated aqueous solutions of NADH at 355 nm (buffered with 10 mM CH_3COOH, pH 5.0). The plasma-formation threshold is reduced to that observed *in vivo* for an NADH concentration of 38 mM. This is higher than the average physiological range; however, NADH is not homogeneously distributed in cells, but is instead concentrated in mitochondria. As for the laser-induced cavitation dynamics, T_{osc} (and R_{max}) are larger in NADH solution than *in vivo*—additional evidence that the biological matrix constrains the cavitation bubbles. As shown in Fig. 3, the curve of T_{osc} versus pulse energy in NADH solution simply extends the in-water curve to lower pulse energies.

In the discussions above, we repeatedly used the Rayleigh formula to calculate R_{max} for each measured T_{osc}. To assess the reliability of this formula under our nonideal conditions, we directly imaged passage of the bubble front. To do so, the ablating laser and the microscope's 647 nm Ar-Kr line are focused to two different spots in the same plane, but separated by a distance r. Using a confocal pinhole and photomultiplier tube, we collect the backscattered 647-nm light. Very little light is normally backscattered, but if the cavitation bubble expands far enough, then the backscattered light increases dramatically as the bubble front passes by (at time t_1), and remains high until the bubble front passes by again during bubble collapse (at time t_2). Each backscattered signal trace yields two points in the curve of bubble radius versus time, i.e., $r(t_1)$ and $r(t_2)$. Multiple ablations at different separation distances are used to construct the entire $r(t)$ curve. Since T_{osc} (and R_{max}) vary from pulse to pulse, times

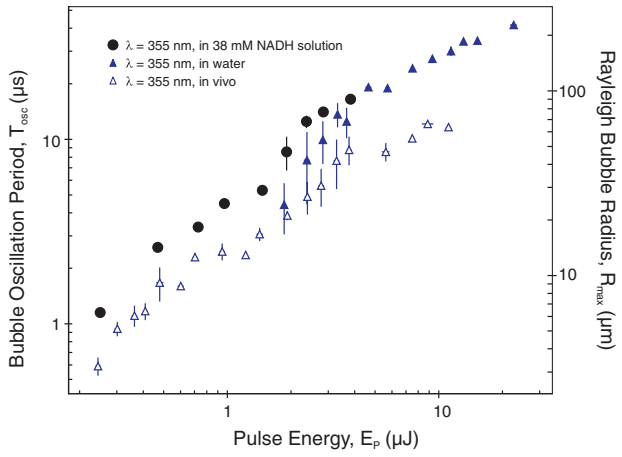

FIG. 3 (color online). Cavitation bubble parameters from 355 nm ablation in water, *in vivo*, and in a 38 mM NADH solution.

are normalized by T_{osc} and distances by R_{max}, as shown in Fig. 4. In distilled water, this procedure traces out a very smooth trajectory with the largest cavitation bubbles reaching radii of $0.86R_{max}$ and with no evidence for bubble passage above $0.93R_{max}$. Thus these bubbles appear to be 7–14% smaller than predicted. The *in vivo* bubble trajectory is not as reproducible. Here we find bubbles reaching radii of $1.16R_{max}$; and there are examples with no evidence for bubble passage as small as $1.11R_{max}$. Thus the *in vivo* bubbles appear to be 11–16% larger than predicted. The differences likely result from the different ways spherical symmetry is broken. Bubbles in water can expand freely away from the coverslip and out of the focal plane. Bubbles *in vivo* are constrained between embryonic tissue layers and can only expand freely within the focal plane.

After confirming the Rayleigh formula as a reasonable approximation *in vivo*, we can use our hydrophone data to estimate shock wave and cavitation bubble energies [10]. These estimates are plotted in Fig. 5 as fractions of the laser pulse energy, E_P. The shock wave energies show little distinction between in-water and *in vivo* data. All points

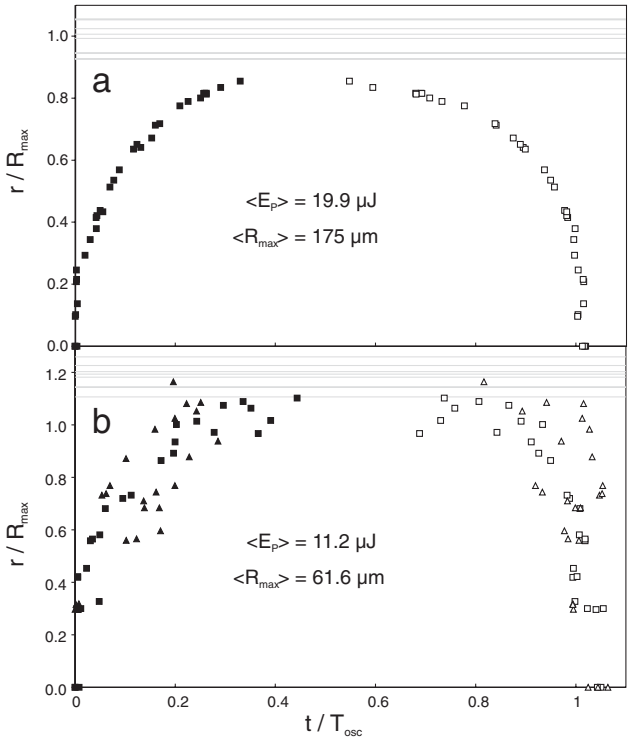

FIG. 4. Direct measurements of the growth and collapse of ablation-induced cavitation bubbles via confocal laser backscatter: (a) in water at 532 nm; and (b) *in vivo* at 532 nm. The average pulse energy, E_P, and calculated R_{max} for each data set are given. Filled symbols represent passage of the bubble front during expansion; open symbols represent the passage during bubble collapse. The gray lines represent distances at which we saw no evidence of bubble passage. For *in vivo* experiments, the separation between the ablation site and the imaging laser is parallel to the long axis (■) or short axis (▲) of the embryo.

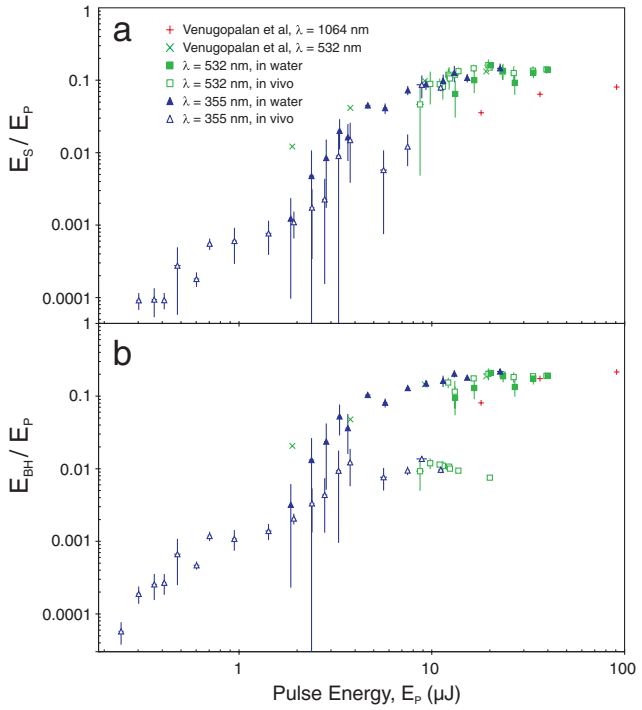

FIG. 5 (color online). Fraction of the laser pulse energy represented in (a) the shock wave at 1.5 mm from the ablation site and (b) maximal expansion of the cavitation bubble against hydrostatic pressure. To facilitate comparison, we have included data previously reported for ablation in water at 532 and 1064 nm [10].

fall along a single trend line that plateaus at 15% of E_P. Since the measured shock waves traveled 1.5 mm from the ablation site, this is a lower bound on the initial shock wave energy. For the cavitation bubble energies, we only calculate the hydrostatic contribution at maximum bubble radius. Just as in the plot of T_{osc}, this plot shows one wavelength-independent curve in water and a different wavelength-independent curve *in vivo*. The hydrostatic contribution to cavitation bubble energy is up to 20% of E_P in water, but just 1% *in vivo*. Considering the similarities in shock wave energies (for a given pulse energy), the initial bubble energies in water and *in vivo* are likely similar. The missing, nonhydrostatic energy *in vivo* is taken up by elastic/plastic deformation of the surrounding biological matrix. At the lowest energies, where ablation is only possible at 355 nm and *in vivo*, the shock wave and expansion of the cavitation bubble against hydrostatic pressure retain less than 0.01% of the laser pulse energy.

In conclusion, these experiments have shown that the size of laser-induced cavitation bubbles is a major determinant of the region disrupted during *in vivo* laser microsurgery. The bubbles induced *in vivo* are much smaller than in water due to two effects: (1) the plasma-formation threshold is greatly reduced at near-UV wavelengths where endogenous chromophores like NADH can serve as alternative, low-intensity sources of seed electrons; and (2) the expansion of cavitation bubbles is constrained by the surrounding matrix. The first effect means that laser microsurgery *in vivo* can be much more precise at near-UV wavelengths. This is certainly true for ns pulses applied to fruit fly embryos. Whether a similar wavelength-dependence holds for ps and fs pulses depends on the crossover intensity at which the multiphoton ionization rate of water surpasses the sequential two-photon ionization of NADH. In any case, optimization of laser microsurgery applications cannot rely solely on extrapolations from water, but must carefully consider both *in vivo* effects.

This work supported by VIIBRE (Vanderbilt Institute for Integrative Biosystem Research & Education) and the National Science Foundation CAREER Program (No. IOB-0545679).

*Corresponding author.
shane.hutson@vanderbilt.edu.

[1] K. O. Greulich *et al.*, J. Microsc. **198**, 182 (2000).
[2] M. W. Berns, W. H. Wright, and R. W. Steubing, Int. Rev. Cytol. **129**, 1 (1991).
[3] J. E. Sulston and J. G. White, Dev. Biol. **78**, 577 (1980).
[4] K. Schutze and G. Lahr, Nat. Biotechnol. **16**, 737 (1998).
[5] W. Tao *et al.*, Proc. Natl. Acad. Sci. U.S.A. **84**, 4180 (1987).
[6] J. Colombelli *et al.*, Traffic **6**, 1093 (2005).
[7] M. S. Hutson, Science **300**, 145 (2003).
[8] M. W. Berns, Biophys. J. **16**, 973 (1976).
[9] P. P. Calmettes and M. W. Berns, Proc. Natl. Acad. Sci. U.S.A. **80**, 7197 (1983).
[10] V. Venugopalan *et al.*, Phys. Rev. Lett. **88**, 078103 (2002).
[11] A. Vogel *et al.*, Appl. Phys. B **81**, 1015 (2005).
[12] D. P. Kiehart *et al.*, in *Cell Biology: A Laboratory Handbook*, edited by J. E. Celis (Academic Press, New York, 2006), pp. 87.
[13] H. Oda and S. Tsukita, Dev. Genes Evol. **209**, 218 (1999).
[14] A. Vogel *et al.*, IEEE J. Sel. Top. Quantum Electron. **2**, 847 (1996).
[15] Lord Rayleigh, Philos. Mag. **34**, 94 (1917).
[16] A. Vogel *et al.*, Appl. Opt. **38**, 3636 (1999).
[17] J. Noack and A. Vogel, IEEE J. Quantum Electron. **35**, 1156 (1999).
[18] K. König, I. Riemann and W. Fritzsche, Opt. Lett. **26**, 819 (2001).
[19] R. G. Wales, Biol. Reprod. **12**, 66 (1975).
[20] B. Chance *et al.*, Science **137**, 499 (1962).
[21] B. Czochralska and L. Lindqvist, Chem. Phys. Lett. **101**, 297 (1983).